HHS Public Access

Author manuscript

J Immunol. Author manuscript; available in PMC 2016 August 15.

Published in final edited form as:

J Immunol. 2015 August 15; 195(4): 1647–1656. doi:10.4049/jimmunol.1500212.

beta-glucuronidase, a regulator of Lyme arthritis severity, modulates lysosomal trafficking and MMP-9 secretion in response to inflammatory stimuli

Kenneth K.C. Bramwell[*], **Kelton Mock**[†], **Ying Ma**[*], **John H. Weis**[*], **Cory Teuscher**[‡], and **Janis J. Weis**[*]

[*] Division of Microbiology and Immunology, Department of Pathology, University of Utah, Salt Lake City, UT 84112

[†] University of Puget Sound, Tacoma, WA 98416

[‡] Department of Medicine, University of Vermont, Burlington, VT 05405

Abstract

The lysosomal enzyme beta-glucuronidase (*Gusb*) is a key regulator of Lyme-associated and K/B×N-induced arthritis severity. The luminal enzymes present in lysosomes provide essential catabolic functions for the homeostatic degradation of a variety of macromolecules. In addition to this essential catabolic function, lysosomes play important roles in the inflammatory response following infection. Secretory lysosomes and related vesicles can participate in the inflammatory response through fusion with the plasma membrane and release of bioactive contents into the extracellular milieu. Here we show that GUSB hypomorphism potentiates lysosomal exocytosis following inflammatory stimulation. This leads to elevated secretion of lysosomal contents, including glycosaminoglycans, lysosomal hydrolases, and Matrix Metalloproteinase 9, a known modulator of Lyme arthritis severity. This mechanistic insight led us to test the efficacy of Rapamycin, a drug known to suppress lysosomal exocytosis. Both Lyme and K/B×N-associated arthritis were suppressed by this treatment concurrent with reduced lysosomal release.

Introduction

Lyme disease is the most prevalent arthropod-borne illness in the United States with over 300,000 estimated cases per year (1). Lyme disease infection occurs following the bite of a tick infected with the spirochete *Borrelia burgdorferi* (2). In a majority of cases, infection leads to the development of an *erythema migrans* “bull’s-eye” rash at the site of the tick bite, which radiates outward along with dissemination of bacteria. Patients experience a wide spectrum of disease symptoms following infection, which are thought to reflect differences in the infectious bacteria as well as in the patients' own unique genetic risk factors. Lyme arthritis is the most prevalent symptom of disseminated infection, observed in 30 to 60 percent of untreated patients (3). While early treatment with appropriate antibiotic therapy often effectively prevents the manifestation of later symptoms associated with disseminated

Corresponding author: Dr. Janis J. Weis, Division of Microbiology and Immunology, Department of Pathology, University of Utah, Address: 15 North Medical Drive, Salt Lake City, UT 84112, Phone: 801-581-8386, Fax: 801-585-7376, janis.weis@path.utah.edu.

infection, up to ten percent of treated patients experience recurrent arthritis symptoms that may persist for months or years (4).

Wild mice and other rodents serve a key role in the enzootic cycle of *B. burgdorferi* in nature (2). Barthold and colleagues made the pivotal observation that inbred strains of laboratory mice exhibit consistent genetic differences in Lyme arthritis severity (5). They observed that C3H mice develop severe Lyme arthritis, while B6 mice experience milder inflammation and pathology, representing opposite ends of the disease spectrum. This observation allowed the influence of underlying host genetic differences to be investigated in a systematic way. Through a forward genetic approach, we recently demonstrated that the lysosomal enzyme beta-glucuronidase (*Gusb*) is a key regulator of Lyme arthritis severity (6). This result was extended to the K/B×N serum transfer model of rheumatoid arthritis, indicating a common role for *Gusb* in these two models of arthritis.

The *Gusb* gene in C3H mice contains a single nucleotide polymorphism that encodes a T87I amino acid substitution and leads to a partial reduction in GUSB enzymatic activity. GUSB is a critical enzyme in the lysosomal pathway used to degrade and recycle glycosaminoglycans (GAGs), and individuals with very severe GUSB deficiencies exhibit spontaneous lysosomal storage of partially degraded GAGs and severe joint/skeletal abnormalities (7). C3H mice do not develop spontaneous lysosome storage symptoms until advanced age, but GUSB hypomorphism does drive substantial arthritogenesis in young mice following challenge with an inflammatory trigger (6). The cellular and molecular mechanisms underlying the observed joint pathogenesis are not fully understood, but the subcellular localization of GUSB to the lysosome and its indispensable enzymatic role implicate alterations in lysosomal function or trafficking as strong candidates for additional investigation.

Materials and Methods

Mice

All mice used in this study were maintained in a pathogen free facility, and cared for in accordance with protocols approved by the University of Utah Institutional Animal Care and Use Committee (IACUC). C57BL/6N (B6) and C3H/HeN (C3H) mice were obtained from the National Cancer Institute and Charles River, respectively. $Gusb^{Null}$ homozygous and heterozygous ($Gusb^{Het}$) mice on a B6 genetic background were originally obtained from Jackson Labs, as described (6). B6.C3H-$Gusb^{h}$ (B6-$Gusb^{h}$) congenic mice were developed as previously described (6), and isolate a C3H-derived locus on Chromosome 5 from 129.0 to 130.5 Mb, containing only one coding polymorphism that is located in the *Gusb* gene, on an otherwise uniform B6 genetic background.

Microscopy

Alcian blue–stained sections were visualized on an Olympus BX41 clinical microscope (Olympus America) using ×4, ×10, or ×40 total magnification. Images were recorded with an Olympus DP72 camera and prepared using Olympus cellSens digital imaging software.

Electron microscopy images were obtained using a JEOL JEM-1400 Plus Transmission Electron Microscope.

LAMP-1 Flow Cytometry Assays

Unelicited resident peritoneal cells were harvested from B6, C3H, and *Gusb*^{Null} littermates as described (8). Cells contained in this naïve peritoneal exudate were resuspended at a concentration of 5×10^5/ml in serum-replacement medium (RPMI 1640 medium (Invitrogen) supplemented with 1% L-glutamine and 1% Nutridoma SP (Roche)) (Control) or serum-replacement medium supplemented with 3% Brewer modified thioglycollate medium (Difco) (3% Thio). 2 ml of cell suspension were aliquoted into 12 × 75 mm Falcon tubes (BD), capped, and incubated in a 37°C water bath for 2 hours. Samples were then washed twice with FACS buffer and stained with 7-aminoactinomycin D for viability discrimination and LAMP-1 PE-conjugated antibody (Clone 1D4B). For lineage discrimination, peritoneal exudate was stained with 4',6-diamidino-2-phenylindole (DAPI) for viability discrimination, and a cocktail of monoclonal antibodies against LAMP-1 AlexaFluor488 (Clone 1D4B), F4/80 APC (Clone BM8), and CD19 BV605 (Clone 6D5). All antibodies were sourced from BioLegend and used at a 1:200 dilution. Sample data were collected on a FACSCanto II (BD) and analyzed using FlowJo v. 9.4.11 software. Live single cells were selected by gating all samples on Forward Scatter Height versus Forward Scatter Width to exclude doublets, and then by subsequently gating out any cells staining positively for 7-AAD or DAPI, respectively (data not shown).

Culture of bone marrow–derived macrophages (BMDM)

BMDM were generated as described (19). BMDM growth medium consisted of RPMI 1640 medium (Invitrogen) supplemented with 30% L929 conditioned medium and 20% horse serum (HyClone). Strain-specific BMDM were harvested, resuspended in serum-replacement medium at a density of 6×10^5/ml, and 500 µl aliquots were replated into 24-well plates and cultured overnight.

Culture of *Borrelia burgdorferi* and BMDM co-incubation

N40 isolate *B. burgdorferi* cells (provided by Stephen Barthold, UCD, Davis, California, USA) were cultured in Barbour-Stoenner-Kelly II medium containing 6% rabbit serum (Sigma-Aldrich). Live *B. burgdorferi* were visualized and counted using a Petroff-Houser counting chamber and a dark-field condenser. An aliquot of *B. burgdorferi* were centrifuged at 6,000g on a tabletop centrifuge for 6 minutes, resuspended in room temperature 1× phosphate buffered saline (PBS), centrifuged again and resuspended in serum-replacement medium at a high concentration of 7.4×10^6/ml, or a low concentration of 7.4×10^5/ml. 24-well plates of strain-specific BMDM were removed from the incubator and the serum-replacement culture medium was aspirated and replaced with 500 µl of either freshly prepared serum-replacement medium, Low concentration *B. burgdorferi* medium, or High concentration *B. burgdorferi* medium, and returned to the incubator. The High and Low concentrations used produce a Multiplicity of Infection of approximately 25 and 2.5, respectively. 24 hours later, supernatants were harvested into individual 1.7 ml microcentrifuge tubes and centrifuged at 6,000g for 6 minutes. 400 µl of the resulting cell-

free supernatants were then transferred into a 96-well 500 µl round bottom assay plate (Axygen). To obtain cell extracts, cells were washed once with 1× PBS, and then incubated in extraction buffer (50 mM $NaPO_4$, pH 7.0; 10 mM BME; 10 mM EDTA; 0.1% sarcosyl; 0.1% Triton X-100) on a rocker plate at 4°C for 30 minutes. Extracts were then homogenized by pipeting up and down, and 400 µl was transferred into a 96-well assay plate.

β-galactosidase (BGAL) enzyme assay

4-Methylumbelliferyl β-D-galactopyranoside (MUGal) (Marker Gene) was used as a fluorogenic substrate to measure BGAL enzymatic activity. 10 µl of sample (serum, cell extract, or supernatant) was incubated with 1 mM MUGal in a total volume of 50 µl assay buffer (100 mM sodium citrate; pH 4.4) for 1 hour at 37°C in a 96-well plate (Costar). 150 µl of stop buffer (200 mM sodium carbonate) was then added, and samples were analyzed on a Biotek Synergy HT microplate reader. Fluorescence was measured with an excitation wavelength of 360 nm and an emission wavelength of 460 nm. Units were calculated by comparison against a standard curve prepared using free 4-Methylumbelliferone (Sigma-Aldrich). Results are expressed as arbitrary units (AU), with the average value of B6 unstimulated control samples within each assay run set at a baseline of 100.

Gelatin Zymography

20 µl of cell-free BMDM supernatant was added to 20 µl of Zymogram Sample Buffer (Bio-Rad) and loaded onto 10% polyacrylamide gels embedded with gelatin (Bio-Rad). Electrophoresis buffer was prepared from a 10× stock solution (15 g Tris base, 72 g Glycine, 5 g Sodium dodecyl sulfate dissolved in 500 ml Milli-Q water). Zymography gels were electrophoresed at 100 Volts for 1 hour. After electrophoresis, gels were removed from the cassette and incubated in 1× Zymogram Renaturation Buffer (Bio-Rad) at room temperature on a rocker plate for 30 minutes, followed by overnight incubation at 37°C in Zymography Development Buffer (Bio-Rad). Gels were then stained with 2.5% Coomassie Blue R-250 (Bio-Rad) dissolved in a solution of 50% methanol, 10% glacial acetic acid, and 50% Milli-Q water for 30 minutes. Gels were destained using 50% methanol, 10% glacial acetic acid, and 50% Milli-Q water, then imaged. Density analysis of the bands was performed using ImageJ. The appropriate position of the MMP-9 zymography band was verified using recombinant mouse MMP-9 (AnaSpec) (data not shown).

Enzyme Linked Immunosorbent Assay

MMP-9 ELISA was performed according to the manufacturer instructions using a Quantikine ELISA Mouse Total MMP-9 kit (R&D Systems). Briefly, microplate strips were placed into a 96-well microplate, and filled with 50 µl of assay diluent. 50 µl of cell-free BMDM supernatants, standards, or control solutions were then added, mixed, and incubated for 2 hours at room temperature. Each well was then aspirated and washed four times with wash buffer. 100 µl of Mouse Total MMP-9 Conjugate was added to each well, covered, and incubated for 2 hours at room temperature. The plate was again aspirated and washed 4 times. 100 µl of substrate solution was added, the plate was covered and incubated at room temperature for 30 minutes in the dark. 100 µl of stop solution was added to each well, and

the plate was read using a Biotek Synergy HT microplate reader at an absorbance of 450 nm and a wavelength correction set to 540 nm.

Rapamycin treatment of mice

Rapamycin (LC Laboratories) was dissolved in EtOH to prepare a 100 mg/ml stock solution. This was diluted to 1.2 mg/ml into a vehicle solution of 1x PBS, 5% PEG-400, and 5% Tween-20. B6-*Gusb*^{h} mice were given daily intraperitoneal injections of either 8 mg/kg Rapamycin or an equivalent volume of Vehicle, beginning two days prior to the initiation of the experimental arthritis protocols and continuing throughout the course of the experiment with the final injection given the day prior to sacrifice.

K/B×N serum transfer experiments

Experiments were carried out as described (6). Briefly, rear ankle joints of mice between 6 and 7 weeks of age were measured with a metric caliper prior to treatment. 100 μl of K/B×N serum was administered by intraperitoneal injections on days 0 and 2. Ankle swelling was determined by caliper measurements on days 5 and 7. After the final day 7 measurements, serum was collected for enzyme assays, the most swollen rear ankle joint was harvested for histological analysis, and the less swollen joint and the spleen were excised, immersed in RNA Later (Qiagen), and stored at -80°C.

B. burgdorferi infection of mice

Mice between 6 and 7 weeks of age were infected by intradermal injection with 2×10^4 bacteria of the *B. burgdorferi* N40 isolate. Sonicated *B. burgdorferi* used for *in vitro* stimulation was prepared as described (9).

Lyme arthritis analysis

Rear ankle joints were measured at the time of infection and at 4 weeks after infection by using a metric caliper, as described (19). Measurements of the thickest anteroposterior portion of the ankle with the joint extended were taken and are reported as the change in ankle swelling over time. For histological evaluation, tissues were fixed in 10% neutral buffered formalin, decalcified, embedded in paraffin, and cut into 3-μm–thick sections; sections were mounted onto glass slides and stained with H&E or with Alcian blue as described (6).

Isolation of RNA and quantitative RT-PCR

Total RNA was recovered from homogenized tissue using TRIzol reagent (Invitrogen). 5 μg of total RNA was reverse transcribed using random primers and Moloney murine leukemia virus RT (Invitrogen). Transcripts were quantified using LightCycler Sybr Plus master mix and a LC-480 PCR system (Roche). The primers used were as follows: *β-actin* forward 5'-GTAACAATGCCATGTTCAAT-3' and reverse 5'-CTCCATCGTGGGCCGCTCTAG-3'; *Glb1* forward 5'-GTGGATAAATGGCTGGCAGT-3' and reverse 5'-TACCCAGATGGTAGCGGAAG-3'.

Results

We previously identified an increased extracellular GAG deposition, visualized histochemically with Alcian blue staining, and localized inflammation following *B. burgdorferi* infection in severely *Gusb* deficient mice on a B6 genetic background ($Gusb^{Null}$) and several *Gusb* hypomorphic strains (6, 10). The previously described runted growth and spontaneous rheumatologic abnormalities of $Gusb^{Null}$ mice suggest that the presence of excess partially degraded GAGs may be responsible for a shared disease process underlying both pathologies (11). Additionally, the results of radiation chimera studies indicated that the *Gusb* genotype of joint resident cells determines the severity of arthritis, suggesting that GAG released by these cells could contribute to localized inflammation. To investigate this, we compared the Alcian blue positive GAG staining patterns of joints from sham injected and *B. burgdorferi* infected B6-$Gusb^{h}$, $Gusb^{Null}$, and $Gusb^{Het}$ littermate control mice. Following *B. burgdorferi* infection, $Gusb^{Het}$, B6-$Gusb^{h}$, and $Gusb^{Null}$ mice develop mild, moderate, and maximal arthritis, respectively (6). The Alcian blue positivity in joints from both sham and infected $Gusb^{Het}$ mice is primarily restricted to the articular surfaces of the cartilage and within the bones of the leg, ankle, and foot (Figure 1). Ankle joints from infected B6-$Gusb^{h}$ mice exhibit extracellular GAG deposition in areas associated with histopathology, and this localized deposition is exaggerated further in $Gusb^{Null}$ mice. Because the cellularity of the cranial-tibial tendon sheath is so widely variable between sham and infected mice, we attempted to focus high magnification (×40) images on an adjacent area that is densely cellular in all samples. The extracellular deposition of these GAGs is most apparent at this high magnification. Although $Gusb^{Null}$ mice are expected to spontaneously accumulate excess GAGs even in the absence of infection (11), we found that joints from sham injected $Gusb^{Null}$ mice exhibit minimal extracellular GAG staining. To quantify intracellular GAG storage, bone marrow-derived macrophages (BMDM) from $Gusb^{Het}$ and $Gusb^{Null}$ mice were prepared and visualized by transmission electron microscopy (Figure 2). As expected, $Gusb^{Null}$ cells exhibited many electron sparse storage vacuoles of irregular size and shape, consistent with a lysosome storage disease phenotype. Together, these data suggest that although *Gusb* deficiency leads to intracellular accumulation of excess GAG, which may have an independent role in arthritogenesis that deserves further study, *Gusb* appears to play a distinct additional role in intracellular vesicular trafficking in response to inflammatory stimuli.

The role of *Gusb* deficiency in lysosomal trafficking was investigated by measuring the amount of the lysosomal integral membrane protein LAMP-1 present on the cell surface following stimulation with the non-specific agonist thioglycollate. Unelicited peritoneal exudates from naïve B6 control mice, as well as $Gusb^{Null}$ and $Gusb^{Het}$ littermate mice, were collected and the cells stimulated *ex vivo* for 2 hours, and analyzed by flow cytometry. We found that unstimulated peritoneal exudate cells from these strains exhibited a uniformly low LAMP-1 baseline condition (Figure 3A and 3B, Control). Thioglycollate treatment of naïve peritoneal cells markedly induced LAMP-1 cell surface staining in all groups, as reflected in an increased percentage of LAMP-1 positive cells and in the elevated mean fluorescence intensity of all single cells (Figure 3A and 3B, +3 % Thio). $Gusb^{Null}$ cells

exhibited significantly greater LAMP-1 cell surface staining than either B6 or *Gusb*^{Het} cells by each of these metrics ($P < 0.001$).

To determine which exudate cell types were responsible for this elevated LAMP-1 positivity, the experiments were repeated using a cocktail of additional cell-type specific antibodies. CD19^{+} B-cells (60-80%) and F4&/80^{+} macrophages (10-25%) comprise the largest percentage of cells in the unelicited peritoneal exudate of naïve mice (data not shown). Under basal conditions, naïve peritoneal macrophages from both *Gusb*^{Het} and *Gusb*^{Null} mice are LAMP-1 positive, while peritoneal B-cells from both strains are predominantly LAMP-1 negative (Figure 3C). Following thioglycollate stimulation, a subset of *Gusb*^{Het} peritoneal macrophages further mobilized LAMP-1 onto the cell surface to adopt a LAMP-1 high phenotype. In contrast, *Gusb*^{Null} peritoneal macrophages almost exclusively adopted a LAMP-1 high phenotype following stimulation, with very few LAMP-1 low cells observed. Stimulated *Gusb*^{Het} peritoneal B-cells exhibited minimal LAMP-1 positivity, but strikingly, a majority of stimulated *Gusb*^{Null} peritoneal B-cells became LAMP-1 positive. These data indicate that severe GUSB deficiency impacts lysosomal trafficking and fusion with the plasma membrane in response to cellular activation in multiple cell types.

Based on previous reports suggesting that *B. burgdorferi* co-incubation induces exocytosis in a variety of myeloid cell types (12), a second experimental approach was pursued to evaluate the impact of *Gusb* hypomorphism on lysosomal exocytosis. BMDM were generated from B6, *Gusb* hypomorphic (B6-*Gusb*^{h}), and C3H mice. Cells were plated overnight, washed, and stimulated by co-incubation with live *Borrelia burgdorferi* in serum-replacement medium. After 24 hours of co-incubation, cell-free supernatants were harvested and analyzed for release of the lysosomal enzyme beta-galactosidase (BGAL) using a fluorogenic enzymatic activity assay. We observed that co-incubation with a high concentration of *B. burgdorferi* was associated with a marked induction of BGAL release into the supernatant by macrophages from all three strains (Figure 4A, HIGH). Interestingly, despite an otherwise shared B6 genetic background, BGAL release by B6-*Gusb*^{h} macrophages following co-incubation was significantly elevated above that of B6 control macrophages. In addition, BGAL activity in corresponding cell extracts was constant across the two strains under basal or stimulated conditions (Figure 4B), suggesting that the observed increase in supernatant activity is not a consequence of bulk changes in cellular BGAL production. Co-incubation with a 10-fold lower concentration of live *B. burgdorferi* (Figure 4A, LOW) triggered considerable BGAL release by BMDM from C3H mice, but not by BMDM from either B6 strain. This confirms the dose dependency of the effect, and indicates that other unidentified genetic differences between B6 and C3H strains also influence this cellular response.

Due to the intriguing effect of severe *Gusb* deficiency on lysosomal trafficking in non-myeloid cells (Figure 3C), we next investigated whether *Gusb* hypomorphism would have a similar impact on fibroblasts, a non-myeloid cell type that is potentially relevant to disease pathogenesis in Lyme and rheumatoid arthritis. We cultured mouse embryonic fibroblasts (MEFs) derived from B6, B6-*Gusb*^{h}, and C3H strains, and measured their levels of BGAL release following 24 hours of co-incubation with live *B. burgdorferi*. B6 control MEFs displayed no significant change in BGAL release following stimulation, while B6-*Gusb*^{h}

MEFs exhibited a significantly elevated BGAL signal ($P < 0.001$)(Figure 4C, D). These data suggest that *Gusb*^{h} allele alone can contribute to elevated lysosomal exocytosis following cell activation in multiple distinct cell types. Interestingly, the increase observed in B6-*Gusb*^{h} was not seen in C3H control MEFs, suggesting that the C3H strain may harbor additional unknown balancing genetic polymorphisms expressed in fibroblasts which stabilize their response to cellular activation.

Although release of BGAL is a reasonable surrogate marker for lysosomal trafficking, it and other related lysosomal enzymes are catalytically inactive at the near neutral pH of the extracellular space, and are therefore unlikely to contribute to pathogenesis in any meaningful way. To investigate a plausible downstream effector, we considered Matrix metalloproteinase 9 (MMP-9). MMP-9 is essential for murine arthritogenesis following *B. burgdorferi* infection (13), and intracellular MMP-9 strongly co-localizes with LAMP-2 positive vesicles by confocal microscopy (14). To determine whether the *Gusb*^{h} allele leads to elevated MMP-9 release, BMDM supernatants obtained after 24 hours of co-incubation with a high dose of 7.4×10^6/ml *B. burgdorferi* were tested for MMP-9 activity by gelatin zymography (Figure 5A). Supernatants from unstimulated B6 and B6-*Gusb*^{h} BMDM exhibited low basal MMP-9 enzymatic activities, which were significantly elevated in samples co-incubated with live *B. burgdorferi.* The MMP-9 activities of co-incubated B6-*Gusb*^{h} supernatants were significantly elevated above those of B6 (Figure 5B, $P < 0.001$). In this assay, C3H-derived BMDM supernatants displayed an elevated basal level of MMP-9 activity, which was further induced by *B. burgdorferi* co-incubation, suggesting that other unknown genetic differences in this strain influence MMP-9 levels. To validate this result with another experimental approach, supernatant MMP-9 protein levels were also evaluated by enzyme linked immunosorbent assay (ELISA) (Figure 5C). Both the elevated basal MMP-9 levels in C3H-derived cells and the exuberant release of MMP-9 associated with the *Gusb*^{h} allele were corroborated by this second approach.

Based on a previous report that Rapamycin treatment suppresses lysosome exocytosis (15), we examined the impact of Rapamycin treatment on BGAL release *in vitro*. MEFs derived from B6-*Gusb*^{h} mice were stimulated with 5 μg/ml sonicated *B. burgdorferi* for 24 hours in serum-replacement medium containing either Vehicle or 100 nM Rapamycin. We found that Rapamycin significantly reduced release of BGAL into supernatants (Figure 6). To determine if transcriptional downregulation could be responsible, transcripts from the beta-galactosidase gene (*Glb1*) were assessed by qRT-PCR. We found that Rapamycin caused no significant change in the abundance of beta-galactosidase transcripts relative to Vehicle treated control samples in MEFs (data not shown).

Next we evaluated the impact of daily Rapamycin treatment on arthritis severity following K/B×N treatment. We observed that K/B×N-treated B6-*Gusb*^{h} congenic mice receiving Rapamycin developed significantly less severe ankle swelling than those treated with Vehicle (Figure 7A, $P < 0.01$). Rapamycin treatment was associated with reduced serum BGAL levels, consistent with inhibition of bulk cellular release (Figure 7B). qRT-PCR analyses of K/B×N-treated mice were conducted at day 7 on spleens as a tissue distant from the inflammatory response and on ankle joints as the primary site of inflammation, and we found that our daily systemic delivery of Rapamycin had no significant impact on the

abundance of beta-galactosidase transcripts in either case (Figure 7C, D). These findings are consistent with our results in MEFs, in which Rapamycin mitigated cellular release of BGAL without altering its transcription. Alcian blue staining was also used to visualize the marked differences in ankle joint histology between mice treated with Rapamycin or Vehicle, as indicated (Figure 7E, F).

Then we evaluated Rapamycin on Lyme arthritis severity following *B. burgdorferi* infection. We observed that B6 control mice developed mild ankle swelling, and that Vehicle treated B6-*Gusb*^{h} congenic mice exhibited significantly more severe arthritis (Figure 8A, $P < 0.05$). However, this elevated ankle swelling was significantly reduced in Rapamycin treated B6-*Gusb*^{h} congenic mice ($P < 0.01$), and this treated group was statistically indistinguishable from our B6 negative controls. Serum BGAL levels of *B. burgdorferi* infected B6-*Gusb*^{h} congenic mice were also significantly suppressed by Rapamycin treatment (Figure 8B). To determine whether Rapamycin treatment influenced the bacterial burden of infected mice, qRT-PCR analysis was conducted on samples prepared from heart tissue. We found that the bacterial burden was significantly higher in Rapamycin treated mice (Figure 8C, $P < 0.0001$), despite their markedly lower arthritis severity (Figure 8A). These data suggest that Rapamycin treatment has important and distinct impacts on host defense and arthritogenesis, although the effective suppression of arthritogenesis conferred by *Gusb* hypomorphism despite elevated bacterial burden is remarkable.

Taken together, these data are consistent with a cellular model whereby GUSB plays distinct but synergistic roles in GAG homeostasis and vesicular trafficking (Figure 9). Under resting conditions, GUSB hypomorphism leads to mild intracellular accumulation of GAGs. In the absence of a second pathological trigger this accumulation remains asymptomatic, but may progress with advancing age (16). Severe GUSB deficiency leads to spontaneous intracellular accumulation of large amounts of GAG in storage vacuoles and induces a spontaneous disease process. Even among individuals carrying identical deficiency mutations, the severity of disease and age of onset may be variable (7). Challenge with an inflammatory trigger leads to lysosomal fusion, cell surface localization of LAMP-1, and exocytosis of MMP-9 and other lysosomal components. In GUSB hypomorphic or deficient cells the magnitude of lysosomal exocytosis is elevated, and this is accompanied by release of intracellular GAGs. These extracellular GAGs are then deposited within the extracellular space, and co-localize with areas of histopathology. Together, these distinct effects of GUSB insufficiency on trafficking and GAG homeostasis shift the normally protective inflammatory response into a pathological cascade. Rapamycin treatment is effective in inhibiting this inflammatory exocytosis, reducing extracellular and serum exoglycosidase levels, and suppressing this pathological cascade. This leads to less severe arthritis in mouse models of both K/B×N-induced and Lyme-associated arthritis, despite the presence of equivalent or even elevated levels of inflammatory stimuli.

Discussion

Our forward genetic approach identified *Gusb* as an unexpected regulator of murine arthritogenesis. The novelty of this discovery has refocused the importance of lysosomes and associated intracellular vesicles in the inflammatory response. The homeostatic

degradation of GAGs by *Gusb* and other closely related lysosomal enzymes is an essential biological process that has primarily been studied in the context of rare, severe congenital enzymatic deficiencies that induce a spontaneous disease process. Although the pathological mechanism by which Lysosomal Storage Diseases (LSD) induce musculoskeletal symptoms is not fully understood, one suggestion is that partially digested substrate fragments may directly activate pro-inflammatory signaling pathways. This idea is bolstered by numerous studies that have demonstrated the therapeutic benefits of anti-inflammatory drugs in animal models of various LSDs (17, 18). These substrates can be detected in the serum and urine of severely affected individuals, and the presence of large excesses or altered relative proportions of distinct GAGs are used for clinical diagnosis (19). This necessitates a pathway for transport out of cellular lysosomes and storage vacuoles, into the extracellular milieu, and eventually into the systemic circulation. However, we observed that extracellular deposition of GAGs in the joint tissue is minimal under basal conditions, even in $Gusb^{Null}$ mice, despite evidence that intracellular GAG accumulation is proceeding as expected (Figures 1, 2). Instead, the extracellular deposition of GAGs appears to be linked to a localized inflammatory response, and is greatly exacerbated in $Gusb^{Null}$ or B6-$Gusb^{h}$ mice. This dichotomy between accumulating excess GAGs intracellularly in the absence of a coincident inflammatory response and depositing GAGs extracellularly during localized pathogenesis strongly infers a role for *Gusb* in vesicular trafficking.

A role for lysosomal trafficking in the pathogenesis of Lyme and rheumatoid arthritis is implied by the elevated levels of lysosomal exoglycosidases, including GUSB and BGAL, in the serum and synovial fluid of patients (20). These levels are reported to be especially high in the synovial fluid of Lyme arthritis patients (21), consistent with a localized response. Alterations in plasma GAG profiles have also been identified in rheumatoid arthritis patients and correlated with the level of ongoing disease activity (22).

Vesicular trafficking is vital to the regulation of cellular inflammatory responses, influencing the expression of adhesion molecules and the release of cytokines, chemokines, ATP, and other effector molecules from a variety of specialized granules, secretory lysosomes, and related vesicles (23, 24). We observed that inflammatory stimuli induce lysosomal exocytosis in peritoneal B-cells, macrophages, and fibroblasts (Figures 3, 4), and this cellular process may be uniformly conserved (25). Lysosomes are a vital source of lipids during plasma membrane repair (26). This repair process is hijacked by the protozoan *Trypanosoma cruzi* to gain entry to the cell (27), and is essential for cellular retention of the parasite (28). Remarkably, C3H inbred mice are highly susceptible to *T. cruzi* infection while B6 mice are resistant, and this C3H susceptibility correlates with exacerbated macrophage activation and cytokine release *in vitro* (29).

In addition to *Gusb*, severe deficiencies in 10 other GAG-degradative lysosomal enzymes (*Idua*, *Ids*, *Gns*, *Hgsnat*, *Naglu*, *Sgsh*, *Galns*, *Glb1*, *Arsb*, *Hyal1*) also result in Mucopolysaccharidosis (MPS I - IX, collectively), and many exhibit musculoskeletal manifestations (30). Severe deficiencies in an additional 8 genes (*Asah1*, *Ctsa*, *Gba*, *Gnptab*, *Gnptg*, *Man2b1*, *Neu1*) linked to lysosomal storage disease of other substrates also produce joint/skeletal manifestations (31). It is noteworthy that among this latter group,

Neuraminidase (*Neu1*) has previously been shown to regulate lysosomal exocytosis (32), suggesting that perhaps other lysosomal enzymes may have a similar effect.

The potentiated release of MMP-9 we observed in *Gusb*^{h} cells following stimulation with live *B. burgdorferi* provides a direct link to a known effector of Lyme arthritogenesis (Figure 5), but also highlights the wide impact that alterations in lysosome exocytosis could have on a variety of pro-inflammatory effectors. In particular, the extracellular release of intracellular GAGs may trigger localized TLR activation (18), modulate cytokine signaling (33, 34), or contribute to the establishment of chemokine gradients (35). These effects are not mutually exclusive, and could all act in concert upon arrival of infectious *Borrelia* in the joint to establish a pro-arthritogenic state (Figure 9).

The mTOR inhibitor Rapamycin has been previously described as a pharmacological inhibitor of lysosomal exocytosis (15). We corroborated these findings *in vitro* and *in vivo*, observing marked reductions of BGAL abundance in cell-free supernatants and serum following Rapamycin treatment. mTOR has been proposed as a potential therapeutic target in clinical osteoarthritis, and this is supported by a correlation between mTOR expression and disease in patients (36) and by preclinical mouse models (37). Introduction of Rapamycin was also reported to induce long-term disease remission in a patient with juvenile rheumatoid arthritis (38). An earlier study found that Rapamycin blunted the development of adjuvant arthritis in rats (39). We found that Rapamycin effectively suppressed the elevated arthritis severity caused by *Gusb* hypomorphism in our mouse models of K/B×N and Lyme arthritis (Figures 7, 8). Because K/B×N arthritis represents the effector phase of disease progression, and because Lyme arthritis severity was reduced despite a marked increase in the bacterial burden of Rapamycin treated animals, this infers that mTOR activation plays an important role in the pathogenic cascade induced by the host response, downstream of the initial inflammatory triggers.

This research has clear implications for human populations, where GUSB levels are widely variable (40, 41). Even more intriguing, the reported elevation of circulating lysosomal enzymes and alterations in GAG profiles within general populations of arthritis patients suggest that lysosomal exocytosis may be a conserved process during inflammatory arthritogenesis, raising its potential diagnostic and therapeutic value. The large impact that GUSB hypomorphism has on experimental arthritis severity and its ubiquitous expression in all cell types infer that lysosomal function and trafficking are important determinants of the pathological trajectory of inflammation following a primary insult.

Acknowledgments

The authors would like to acknowledge Robert Lochhead and Lynn Sonderegger for providing helpful discussions and suggestions, Katie Bashant, Ky-phuong Luong and Anne Brogdon for sample preparation and technical assistance, and Jackie Paquette and Sarah Whiteside for reviewing the manuscript. Electron microscopy was performed by Nancy Chandler at the University of Utah Electron Microscopy Core Laboratory.

Grant Support:

This work was supported by National Institutes of Health/National Institute of Allergy and Infectious Disease Grants T32AI055434 (to K.K.C.B.) and AI32223 (to J.J.W.), National Institutes of Health/National Institute of Arthritis and Musculoskeletal and Skin Diseases Grant AR43521 (to C.T. and J.J.W.), and Arthritis Foundation Grant 6133 (to K.K.C.B.). The DNA/Peptide Core is supported by Cancer Center Support Grant P30 CA04201.

References

1. Kuehn BM. CDC estimates 300,000 US cases of Lyme disease annually. Jama. 2013; 310:1110. [PubMed: 24045727]
2. Radolf JD, Caimano MJ, Stevenson B, Hu LT. Of ticks, mice and men: understanding the dual-host lifestyle of Lyme disease spirochaetes. Nat Rev Microbiol. 2012; 10:87–99. [PubMed: 22230951]
3. Steere AC, Schoen RT, Taylor E. The clinical evolution of Lyme arthritis. Ann Intern Med. 1987; 107:725–731. [PubMed: 3662285]
4. Shapiro ED, Dattwyler R, Nadelman RB, Wormser GP. Response to meta-analysis of Lyme borreliosis symptoms. Int J Epidemiol. 2005; 34:1437–1439. author reply 1440-1433. [PubMed: 16319106]
5. Barthold SW, Beck DS, Hansen GM, Terwilliger GA, Moody KD. Lyme borreliosis in selected strains and ages of laboratory mice. J Infect Dis. 1990; 162:133–138. [PubMed: 2141344]
6. Bramwell KK, Ma Y, Weis JH, Chen X, Zachary JF, Teuscher C, Weis JJ. Lysosomal beta-glucuronidase regulates Lyme and rheumatoid arthritis severity. J Clin Invest. 2014; 124:311–320. [PubMed: 24334460]
7. Tomatsu S, Montano AM, Dung VC, Grubb JH, Sly WS. Mutations and polymorphisms in GUSB gene in mucopolysaccharidosis VII (Sly Syndrome). Hum Mutat. 2009; 30:511–519. [PubMed: 19224584]
8. Ray A, Dittel BN. Isolation of mouse peritoneal cavity cells. J Vis Exp. 2010
9. Ma Y, Seiler KP, Tai KF, Yang L, Woods M, Weis JJ. Outer surface lipoproteins of Borrelia burgdorferi stimulate nitric oxide production by the cytokine-inducible pathway. Infect Immun. 1994; 62:3663–3671. [PubMed: 7520417]
10. Bramwell KK, Teuscher C, Weis JJ. Forward genetic approaches for elucidation of novel regulators of Lyme arthritis severity. Front Cell Infect Microbiol. 2014; 4:76. [PubMed: 24926442]
11. Vogler C, Levy B, Galvin N, Sands MS, Birkenmeier EH, Sly WS, Barker J. A novel model of murine mucopolysaccharidosis type VII due to an intracisternal a particle element transposition into the beta-glucuronidase gene: clinical and pathologic findings. Pediatr Res. 2001; 49:342–348. [PubMed: 11228259]
12. Gebbia JA, Coleman JL, Benach JL. Borrelia spirochetes upregulate release and activation of matrix metalloproteinase gelatinase B (MMP-9) and collagenase 1 (MMP-1) in human cells. Infect Immun. 2001; 69:456–462. [PubMed: 11119537]
13. Heilpern AJ, Wertheim W, He J, Perides G, Bronson RT, Hu LT. Matrix metalloproteinase 9 plays a key role in lyme arthritis but not in dissemination of Borrelia burgdorferi. Infect Immun. 2009; 77:2643–2649. [PubMed: 19364840]
14. Sbai O, Ould-Yahoui A, Ferhat L, Gueye Y, Bernard A, Charrat E, Mehanna A, Risso JJ, Chauvin JP, Fenouillet E, Rivera S, Khrestchatisky M. Differential vesicular distribution and trafficking of MMP-2, MMP-9, and their inhibitors in astrocytes. Glia. 2010; 58:344–366. [PubMed: 19780201]
15. Martins RM, Alves RM, Macedo S, Yoshida N. Starvation and rapamycin differentially regulate host cell lysosome exocytosis and invasion by Trypanosoma cruzi metacyclic forms. Cell Microbiol. 2011; 13:943–954. [PubMed: 21501360]
16. Yatziv S, Erickson RP, Sandman R, Robertson WV. Glycosaminoglycan accumulation with partial deficiency of beta-glucuronidase in the C3H strain of mice. Biochem Genet. 1978; 16:1079–1084. [PubMed: 109077]
17. Eliyahu E, Wolfson T, Ge Y, Jepsen KJ, Schuchman EH, Simonaro CM. Anti-TNF-alpha therapy enhances the effects of enzyme replacement therapy in rats with mucopolysaccharidosis type VI. PLoS One. 2011; 6:e22447. [PubMed: 21887218]
18. Simonaro CM, Ge Y, Eliyahu E, He X, Jepsen KJ, Schuchman EH. Involvement of the Toll-like receptor 4 pathway and use of TNF-alpha antagonists for treatment of the mucopolysaccharidoses. Proc Natl Acad Sci U S A. 2010; 107:222–227. [PubMed: 20018674]
19. Lehman TJ, Miller N, Norquist B, Underhill L, Keutzer J. Diagnosis of the mucopolysaccharidoses. Rheumatology (Oxford). 2011; 50(Suppl 5):v41–48. [PubMed: 22210670]

20. Pancewicz SA, Wielgat P, Hermanowska-Szpakowicz T, Kondrusik M, Zajkowska J, Grygorczuk S, Popko J, Zwierz K. Activity of lysosomal exoglycosidases in the serum of patients with chronic Lyme arthritis. Int J Med Microbiol. 2006; 296(Suppl 40):280–282. [PubMed: 16584916]
21. Pancewicz S, Popko J, Rutkowski R, Knas M, Grygorczuk S, Guszczyn T, Bruczko M, Szajda S, Zajkowska J, Kondrusik M, Sierakowski S, Zwierz K. Activity of lysosomal exoglycosidases in serum and synovial fluid in patients with chronic Lyme and rheumatoid arthritis. Scand J Infect Dis. 2009; 41:584–589. [PubMed: 19513935]
22. Jura-Poltorak A, Komosinska-Vassev K, Kotulska A, Kucharz EJ, Klimek K, Kopec-Medrek M, Olczyk K. Alterations of plasma glycosaminoglycan profile in patients with rheumatoid arthritis in relation to disease activity. Clin Chim Acta. 2014; 433:20–27. [PubMed: 24607326]
23. Appelqvist H, Waster P, Kagedal K, Ollinger K. The lysosome: from waste bag to potential therapeutic target. J Mol Cell Biol. 2013; 5:214–226. [PubMed: 23918283]
24. Wernersson S, Pejler G. Mast cell secretory granules: armed for battle. Nat Rev Immunol. 2014; 14:478–494. [PubMed: 24903914]
25. Rodriguez A, Webster P, Ortego J, Andrews NW. Lysosomes behave as Ca2=-regulated exocytic vesicles in fibroblasts and epithelial cells. J Cell Biol. 1997; 137:93–104. [PubMed: 9105039]
26. Andrews NW, Almeida PE, Corrotte M. Damage control: cellular mechanisms of plasma membrane repair. Trends Cell Biol. 2014
27. Tardieux I, Webster P, Ravesloot J, Boron W, Lunn JA, Heuser JE, Andrews NW. Lysosome recruitment and fusion are early events required for trypanosome invasion of mammalian cells. Cell. 1992; 71:1117–1130. [PubMed: 1473148]
28. Andrade LO, Andrews NW. Lysosomal fusion is essential for the retention of Trypanosoma cruzi inside host cells. J Exp Med. 2004; 200:1135–1143. [PubMed: 15520245]
29. Russo M, Starobinas N, Ribeiro-Dos-Santos R, Minoprio P, Eisen H, Hontebeyrie-Joskowicz M. Susceptible mice present higher macrophage activation than resistant mice during infections with myotropic strains of Trypanosoma cruzi. Parasite Immunol. 1989; 11:385–395. [PubMed: 2528710]
30. Morishita K, Petty RE. Musculoskeletal manifestations of mucopolysaccharidoses. Rheumatology (Oxford). 2011; 50(Suppl 5):v19–25. [PubMed: 22210666]
31. Aldenhoven M, Sakkers RJ, Boelens J, de Koning TJ, Wulffraat NM. Musculoskeletal manifestations of lysosomal storage disorders. Ann Rheum Dis. 2009; 68:1659–1665. [PubMed: 19822711]
32. Yogalingam G, Bonten EJ, van de Vlekkert D, Hu H, Moshiach S, Connell SA, d'Azzo A. Neuraminidase 1 is a negative regulator of lysosomal exocytosis. Dev Cell. 2008; 15:74–86. [PubMed: 18606142]
33. Yoshioka Y, Kozawa E, Urakawa H, Arai E, Futamura N, Zhuo L, Kimata K, Ishiguro N, Nishida Y. Suppression of hyaluronan synthesis alleviates inflammatory responses in murine arthritis and in human rheumatoid synovial fibroblasts. Arthritis Rheum. 2013; 65:1160–1170. [PubMed: 23335273]
34. Petrey AC, de la Motte CA. Hyaluronan, a crucial regulator of inflammation. Front Immunol. 2014; 5:101. [PubMed: 24653726]
35. Johnson Z, Proudfoot AE, Handel TM. Interaction of chemokines and glycosaminoglycans: a new twist in the regulation of chemokine function with opportunities for therapeutic intervention. Cytokine & Growth Factor Reviews. 2005; 16:625–636. [PubMed: 15990353]
36. Tchetina EV, Poole AR, Zaitseva EM, Sharapova EP, Kashevarova NG, Taskina EA, Alekseeva LI, Semyonova LA, Glukhova SI, Kuzin AN, Makarov MA, Makarov SA. Differences in Mammalian target of rapamycin gene expression in the peripheral blood and articular cartilages of osteoarthritic patients and disease activity. Arthritis. 2013; 2013:461486. [PubMed: 23864948]
37. Pal B, Endisha H, Zhang Y, Kapoor M. mTOR: A Potential Therapeutic Target in Osteoarthritis? Drugs R D. 2015; 15:27–36. [PubMed: 25688060]
38. Foroncewicz B, Mucha K, Paczek L, Chmura A, Rowinski W. Efficacy of rapamycin in patient with juvenile rheumatoid arthritis. Transpl Int. 2005; 18:366–368. [PubMed: 15730500]

39. Carlson RP, Hartman DA, Tomchek LA, Walter TL, Lugay JR, Calhoun W, Sehgal SN, Chang JY. Rapamycin, a potential disease-modifying antiarthritic drug. J Pharmacol Exp Ther. 1993; 266:1125–1138. [PubMed: 8355184]

40. Lombardo A, Bairati C, Goi G, Roggi C, Maccarini L, Bollini D, Burlina A. Plasma lysosomal glycohydrolases in a general population. Clin Chim Acta. 1996; 247:39–49. [PubMed: 8920225]

41. Sperker B, Murdter TE, Schick M, Eckhardt K, Bosslet K, Kroemer HK. Interindividual variability in expression and activity of human beta-glucuronidase in liver and kidney: consequences for drug metabolism. J Pharmacol Exp Ther. 1997; 281:914–920. [PubMed: 9152401]

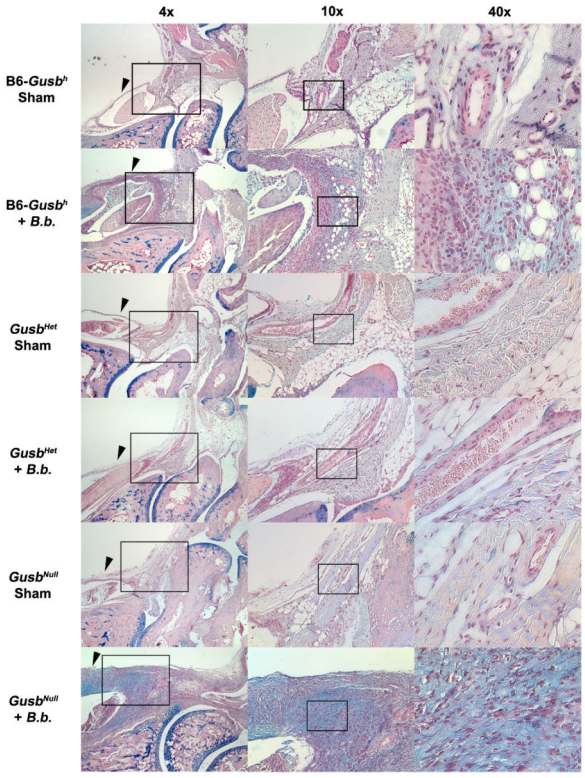

Figure 1. GUSB insufficiency is associated with localized extracellular accumulation of glycosaminoglycans following infection

Representative light microscopy images of Alcian blue stained rear ankle joint sections from sham injected (Sham) or *B. burgdorferi* infected *(+ B.b.)* mice. In each 4× total magnification image, the cranial-tibial tendon is identified with a black arrowhead. Black rectangles indicate the area selected for higher magnification in adjacent images, with total magnifications of 10× and 40×, respectively. Notably, $Gusb^{Null}$ joints do not exhibit extensive extracellular GAG deposition in the absence of infection.

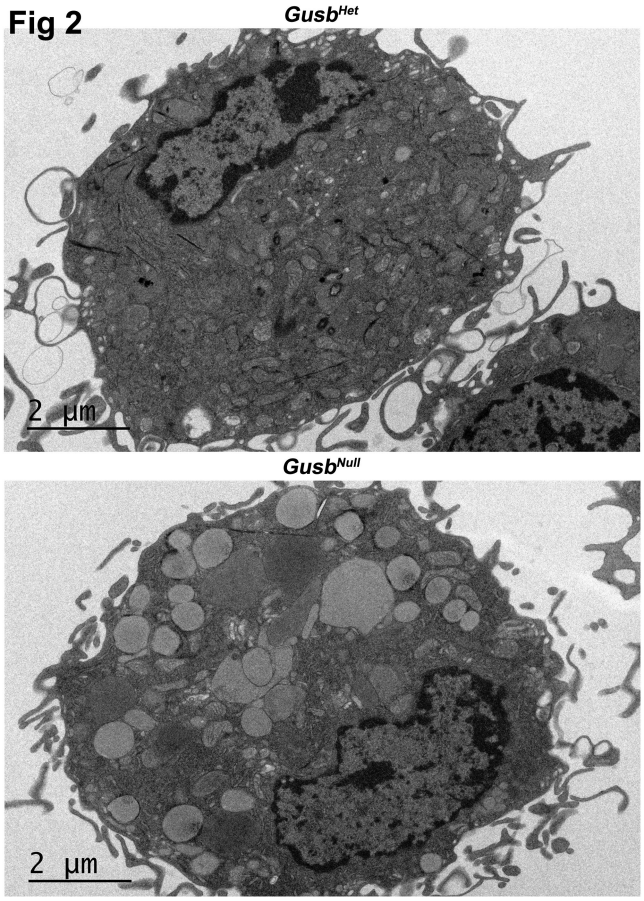

Figure 2. Severe GUSB deficiency is associated with intracellular storage vacuolation under basal conditions

Representative transmission electron micrographs of BMDM produced from *Gusb*^{Het} or *Gusb*^{Null} littermates. *Gusb*^{Null} cells exhibit many electron sparse storage vacuoles of irregular size and shape, consistent with a lysosome storage disease phenotype.

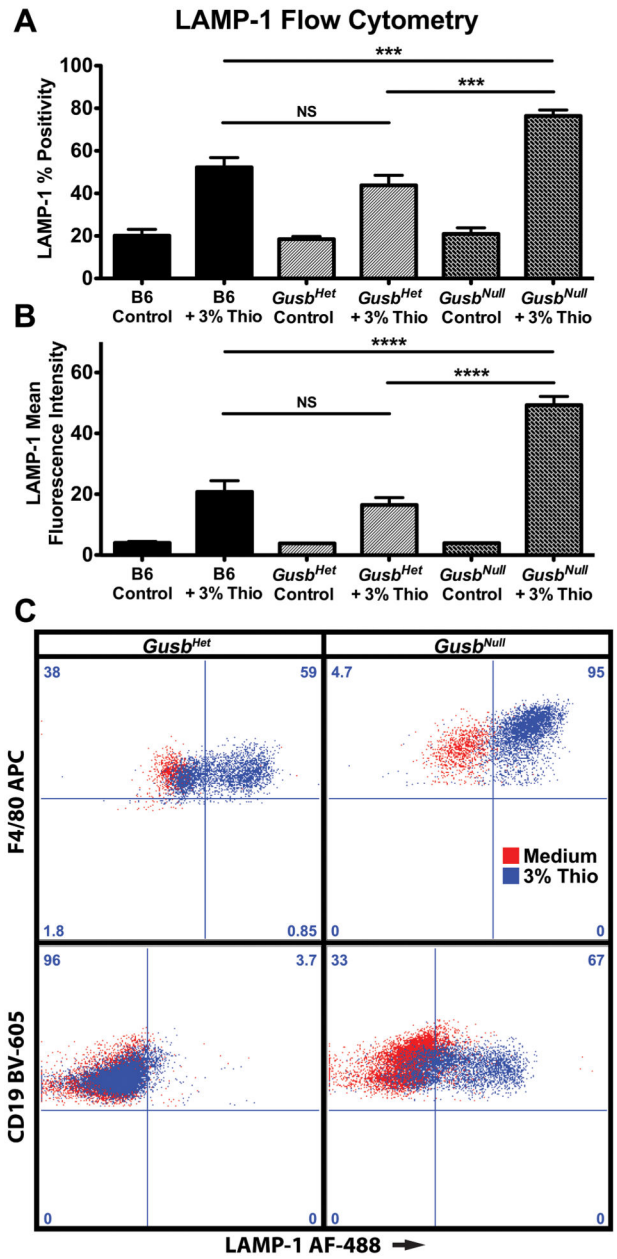

Figure 3. Severe GUSB deficiency is associated with exuberant lysosomal exocytosis following stimulation in multiple cells types

Naïve peritoneal exudate cells from B6, *Gusb*^{Het}, or *Gusb*^{Null} mice were maintained *ex vivo* in serum-replacement medium (Control) or in medium with 3% thioglycollate (+ 3% Thio) for 2 hr, then washed and analyzed by flow cytometry. Cell surface LAMP-1 positivity was measured by the percentage of LAMP-1 positive cells (A) and by the mean fluorescence intensity of all single cells (B). Significance assessed by one-way ANOVA followed by Bonferroni's multiple comparison test (pooled data from 3 independent experiments, n = 3 to 9 samples per group, overall P value < 0.0001). (*** P < 0.001, **** P < 0.0001) (C) Overlay of representative flow cytometry plots of stimulated (3% Thio, Blue) and unstimulated (Medium, Red) peritoneal exudate obtained from *Gusb*^{Het} (left column) or

Gusb^{Null} (right column) mice. Numbers at each corner of the flow cytometry plots represent the percentage of stimulated cells located in each quadrant. The LAMP-1 horizontal axis for all four plots are on an equivalent scale. Quadrants for F4/80-positive peritoneal macrophages (top row) are drawn to separate LAMP-1 Low from LAMP-1 High cells. Quadrants for CD19-positive peritoneal B-bells (bottom row) are drawn to separate LAMP-1 Negative from LAMP-1 Positive cells.

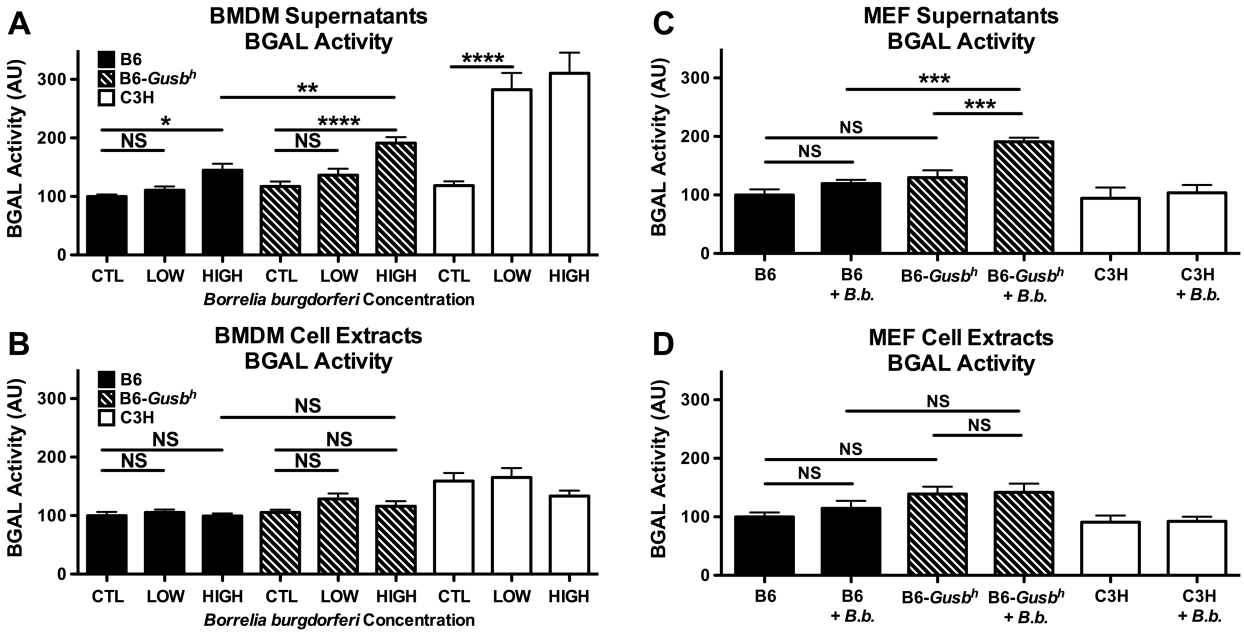

Figure 4. GUSB hypomorphism is associated with exuberant lysosomal exocytosis following stimulation in multiple cell types

BMDM from B6, B6-*Gusb*^{h}, and C3H strains were cultured for 24 hours in the absence or presence of either a LOW (7.4×10^5/ml) or HIGH (7.4×10^6/ml) concentration of live *B. burgdorferi*. Lysosomal exocytosis was evaluated by testing cell-free supernatants (A) and cell extracts (B) for beta-galactosidase (BGAL) activity (pooled triplicate samples from 3 independent experiments, n = 9 samples per group, overall P value < 0.001). Notably, exocytosis is significantly induced by the LOW concentration in C3H BMDM (P < 0.0001, Student's t-test), but not in the two strains on a B6 genetic background. Cell-free supernatants (C) and cell extracts (D) from mouse embryonic fibroblasts were evaluated in a similar manner using HIGH *B. burgdorferi* concentration (pooled triplicate samples from 2 independent experiments, n = 6 samples per group, overall P value < 0.0001) Significance assessed by one-way ANOVA followed by Bonferroni's multiple comparison test of all B6 and B6-*Gusb*^{h} samples. (* P < 0.05, ** P < 0.01, *** P < 0.001, **** P < 0.0001)

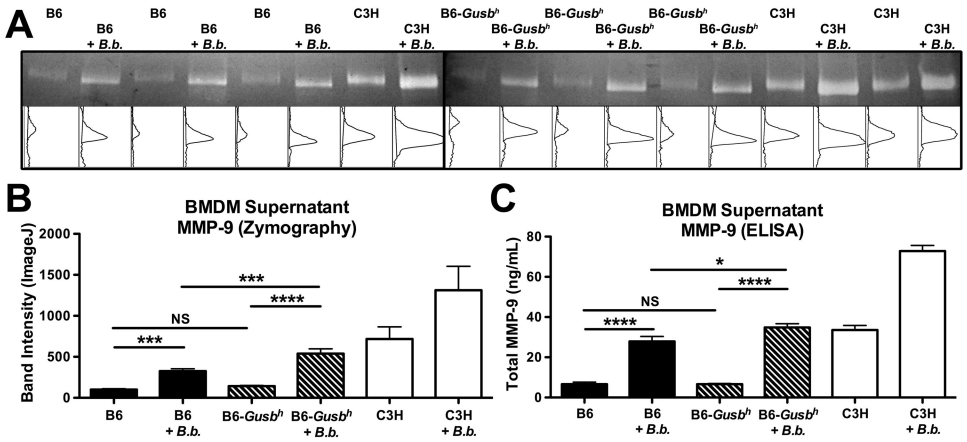

Figure 5. GUSB hypomorphism is associated with elevated MMP-9 release following stimulation

(A) Gelatin zymography for MMP-9 enzyme activity, using cell-free supernatants from B6, B6-*Gusb*^{h}, and C3H BMDM, with or without co-incubation with live *B. burgdorferi* (+ *B.b.*). Upper panel shows two adjacent zymography gels representative of three independent experiments, lower panel shows the ImageJ band densitometry traces used for quantitation. (B) Statistical comparison of gelatin zymography data (pooled triplicate samples from 3 independent experiments, n = 9 samples per group, overall P value < 0.0001) (C) MMP-9 protein levels of cell-free BMDM supernatants, evaluated by enzyme linked immunosorbent assay (ELISA) (pooled triplicate samples from 2 independent experiments, n=6 samples per group, overall P value < 0.0001). Significance assessed by one-way ANOVA followed by Bonferroni's multiple comparison test of all B6 and B6-*Gusb*^{h} samples. (* P < 0.05, *** P < 0.001, **** P < 0.0001)

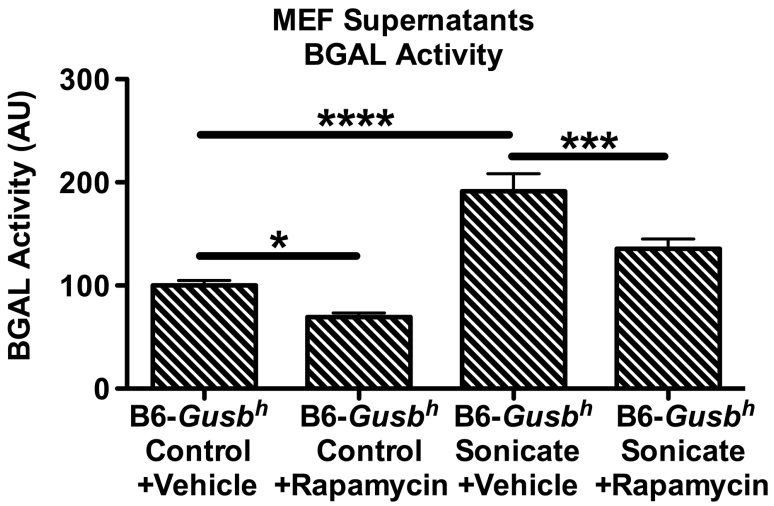

Figure 6. Rapamycin reduces lysosomal exocytosis *in vitro*

MEFs derived from B6-*Gusb*^{h} mice were cultured for 24 hours in the absence or presence of 5 μg/ml sonicated *B. burgdorferi*. During the same 24 hour period, samples were treated with 100 nM Rapamycin or an equivalent volume of vehicle. Statistical analysis of BGAL activity in cell-free supernatants (pooled samples from 2 independent experiments, n = 9 or 12 samples per group, overall P value < 0.0001). Significance assessed by one-way ANOVA followed by Bonferroni's multiple comparison test. (* P < 0.05, *** P < 0.001, **** P < 0.0001)

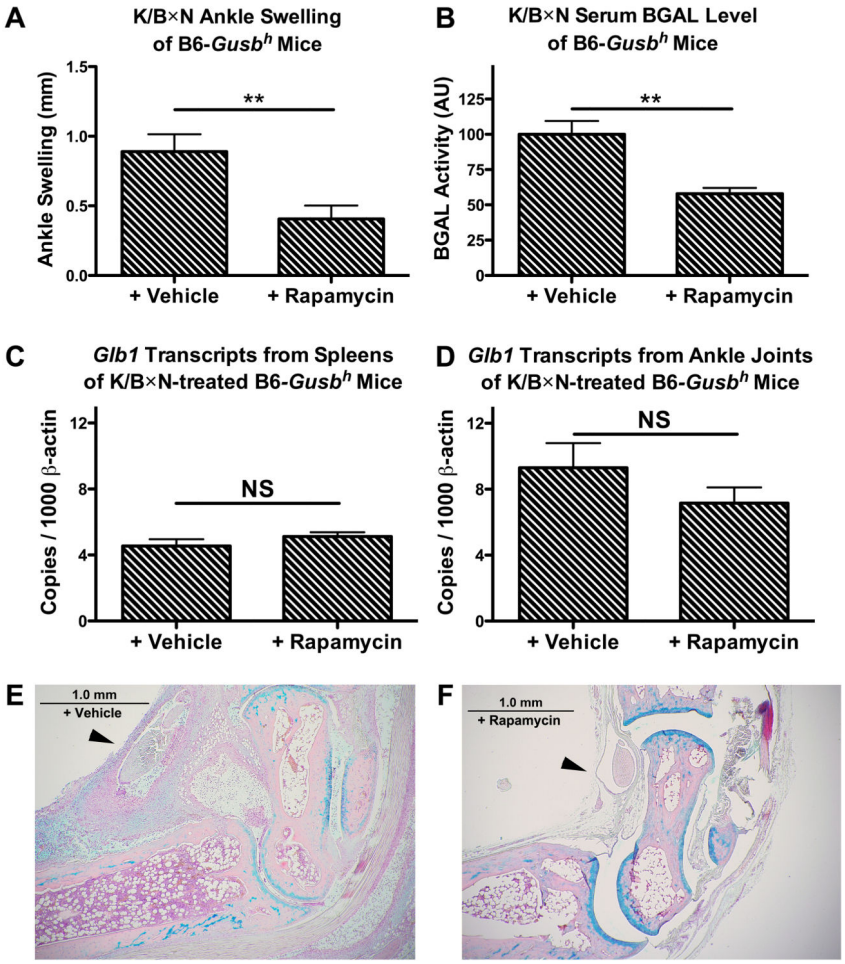

Figure 7. Rapamycin treatment reduces K/B×N-associated ankle swelling

100 μl K/B×N serum was administered to B6-*Gusb*^{h} congenic mice by intraperitoneal injection on days 0 and 2. Mice received daily doses of 8 mg/kg Rapamycin or an equivalent volume of Vehicle, beginning 2 days prior to the first serum injection. (A) The influence of Rapamycin treatment on K/B#x00D7;N-associated ankle swelling at day 7. (n = both rear ankles from 8 mice per group) (B) Serum BGAL activity at day 7 of K/B×N-treated mice administered Vehicle or Rapamycin (n = 8 mice per group). (C) and (D) beta-galactosidase mRNA transcript levels from Spleens or Ankle Joints, respectively. (E) and (F) Alcian blue stained histology slides from K/B×N-treated B6-*Gusb*^{h} mice administered Vehicle or Rapamycin, as indicated. Arrowheads indicate position of the cranial tibial tendon sheath. Significance assessed by unpaired Student's t-test. (* $P < 0.05$, ** $P < 0.01$)

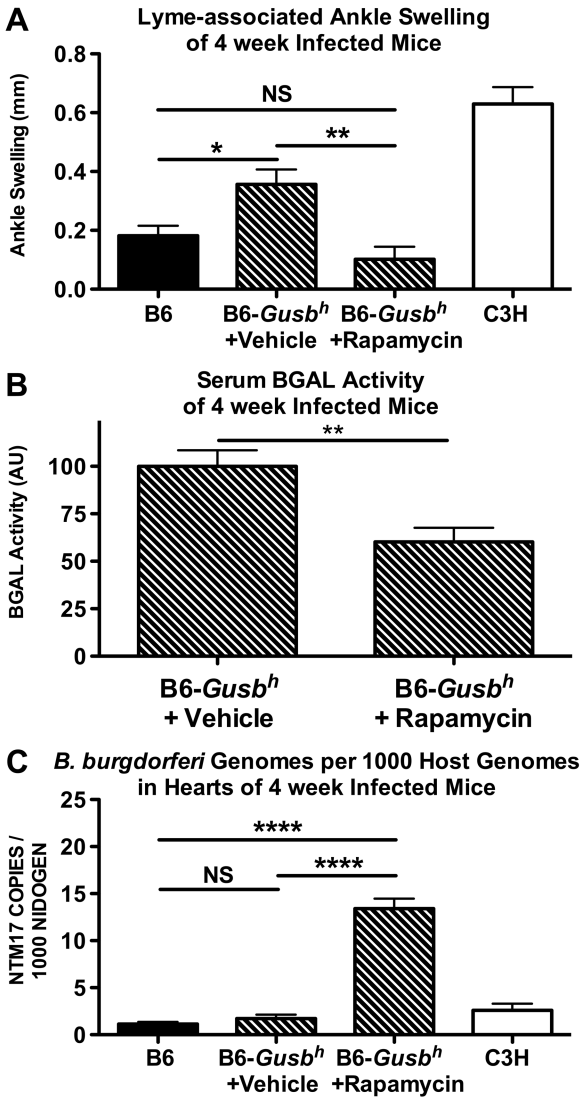

Figure 8. Rapamycin treatment reduces Lyme-associated ankle swelling

(A) Lyme-associated ankle swelling measurements of B6-*Gusb*^{h} mice administered Vehicle or 8 mg/kg Rapamycin daily by intraperitoneal injection, and WT B6 and C3H controls (n = both rear ankles from 4 to 5 mice per group; overall P = 0.0002). (B) Influence of Rapamycin treatment on serum BGAL activity detected at 4 weeks of infection (n = 4 to 5 mice per group). (C) *B. burgdorferi* burden of hearts isolated from B6-*Gusb*^{h} mice administered Vehicle or Rapamycin, and WT B6 and C3H controls (n = 4 to 5 mice per group). Significance assessed by one-way ANOVA followed by Bonferroni's multiple comparison test of all B6 background mice (A and C), or by unpaired Student's t-test (B). (* P < 0.05, ** P < 0.01, **** P < 0.0001)

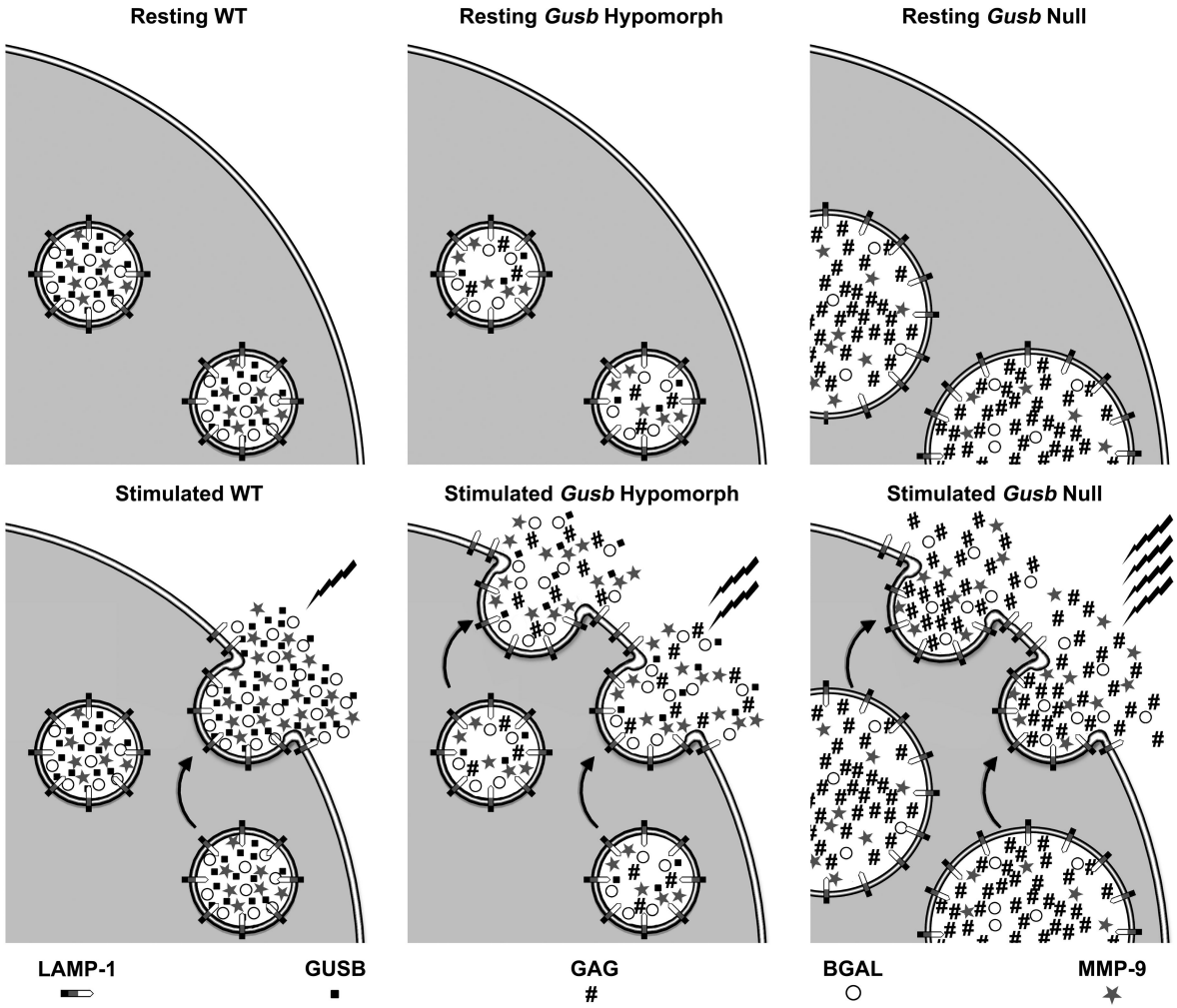

Figure 9. Model of alterations in lysosomal composition and trafficking related to *Gusb* genotype

Upper panels depict homeostatic changes in lysosomal composition determined by lysosomal GUSB levels. Lower panels depict alterations in cellular response following inflammatory stimulation. In resting cells, LAMP-1 is predominantly localized to lysosomal membranes, with GUSB, BGAL, and MMP-9 proteins sequestered within intracellular vesicles. Resting *Gusb* hypomorphic cells develop mild lysosomal GAG storage, with spontaneous formation of enlarged GAG storage vesicles in $Gusb^{Null}$ deficient cells. Inflammatory stimuli induce lysosomal fusion and release of lysosomal contents in all groups. *Gusb* hypomorphism or deficiency each increase the amount of lysosomal fusion following stimulation, as detected by measuring BGAL and MMP-9 release, or LAMP-1 cell surface staining, respectively. These alterations in lysosomal trafficking and composition contribute to downstream inflammatory responses, culminating in altered Lyme and rheumatoid arthritis severity (lightning bolts).